https://doi.org/10.5194/essd-2026-32
Preprint. Discussion started: 3 March 2026

Open Access Earth System Science Data Discussions

Dataset of a 4 km combined seismic and electric streamer survey along the embankment of the Po river in Crescentino.

Cesare Comina[1], Andrea Vergnano[1], Alessandro Arato[2], Emanuele Duò[2], Mario Naldi[2], Dario Chieppa[3] and Laura Valentina Socco[3,4]

[1]Department of Earth Sciences, University of Turin, Italy.
[2] Techgea S.r.l., Italy.
[3]Department of Environment, Land and Infrastructure Engineering, Polytechnic University of Turin, Italy.
[4]Department of Civil Engineering and Geosciences, TU Delft, Netherlands.

ABSTRACT

For river embankment characterization non-invasive geophysical investigations are a valuable complementary tool to standard geotechnical testing. To this aim, resistivity and seismic methods are often adopted and can offer complementary information with respect to pore fluid properties and solid skeleton characteristics, respectively. The use of streamer cables for these surveys can reduce the acquisition times, making geophysical investigations ideal for preliminary screening. Few examples of combined seismic and electric streamer systems were already proposed in the literature, but their applicability for long and extensive surveys still need to be demonstrated. Moreover, tailored processing and interpretation methods are necessary given the large amount of data collected with such systems, which can be challenging for standard processing and inversion software.

We present a dataset of a 4 km combined seismic and electric streamer survey acquired along the embankment of the Po River in Crescentino, near Torino, in north-west Italy. Data acquisition strategies are discussed and preliminary data analyses are reported. The survey demonstrated the efficiency and potentiality of combined seismic and electric streamer systems in investigating river embankments. All the acquired geophysical data, together with complementary geotechnical and topographic information, are made available in a structured dataset (https://doi.org/10.5281/zenodo.18183049). The presented dataset can be an ideal playground to test and benchmark alternative processing and interpretation approaches, and enable an advancement in the state-of-the-art of these characterization methodologies.

Keywords: river embankments, streamer cables, resistivity surveys, seismic surveys, geophysical characterization.

Correspondence:

Cesare Comina
Department of Earth Sciences
University of Turin
cesare.comina@unito.it

Laura Valentina Socco
Department of Civil Engineering and Geosciences
TU Delft
L.V.Socco@tudelft.nl

https://doi.org/10.5194/essd-2026-32
Preprint. Discussion started: 3 March 2026

1 INTRODUCTION

Geotechnical characterization surveys of river embankments, performed with localized geotechnical investigations through drilling or penetration tests, are usually costly and time consuming and provide only local information. Non-invasive geophysical investigations can be complementary to geotechnical testing and provide an efficient characterization of the whole embankment allowing also the number of geotechnical tests to be optimized.

Among the available geophysical methods, the ones based on electrical resistivity (ρ) and seismic velocities (mainly shear wave velocity, Vs) have been the most adopted. They offer complementary information with respect to the pore fluid properties (resistivity methods) and the solid skeleton characteristics (seismic methods). Moreover, relevant geotechnical parameters for the evaluation of the stability of embankments and their efficiency (i.e. hydraulic conductivity, porosity, clay content and others) can be potentially obtained through specific correlations applied to these geophysical data combined (e.g. Vagnon et al. 2022a and b).

Recently, new acquisition approaches with the use of streamer cables have shown to strongly reduce the acquisition times, making geophysical surveys ideal for a preliminary screening. Seismic surveys can be efficiently carried out with seismic streamers, dragged along the embankments. Numerous successful case studies have been presented during the last three decades (e.g. Van Der Veen et al. 2001; Ivanov et al. 2006; Moura and Senos Matias 2012; Comina et al. 2020a), making this acquisition procedure a well-established methodology. On these data, the multichannel analysis of surface waves (MASW), based on the Rayleigh wave dispersion curve (DC) analysis, is considered the most effective for the determination of Vs profiles (Foti et al. 2018). Several Vs profiles are normally estimated along the embankment to generate a pseudo 2D representation of the Vs field. Several applications of this methodology to embankments, river dykes and earth dams are available in literature (e.g. Lutz et al. 2011; Lane et al. 2008; Min and Kim 2006; Comina et al. 2020a).

Conversely, electrical resistivity surveys usually require the insertion of electrodes into the ground, reducing their efficiency and making the acquisition of datasets over long acquisition lines extremely time consuming. Alternative approaches based on Electro Magnetic (EM) methodologies (e.g. frequency or time domain EM) avoid the use of

https://doi.org/10.5194/essd-2026-32
Preprint. Discussion started: 3 March 2026

electrodes but rarely allow a comparable detail in the imaged resistivity distribution. To speed up electrical resistivity surveys few examples of electric streamer cables (e.g. Comina et al. 2020b; Umezawa et al. 2022) or combined seismic and electric streamers systems (e.g. Arato et al. 2022) were already proposed in the literature, but their applicability for long and extensive surveys still need to be demonstrated. The main criticalities of these systems is the electric ground coupling that plays an important role in the data quality. Resistivity interpretation usually rely on tomographic inversion of the acquired data (Electric Resistivity Tomography - ERT) that has proved effective to locate fissures and desiccation cracks (e.g. Jones et al. 2014; An et al. 2020), detect animal burrows (e.g. Borgatti et al. 2017), detect seepages and leakage problems (e.g. Al-Fares 2014; Busato et al. 2016; Lee et al. 2020), monitor water saturation (e.g. Arosio et al. 2017; Tresoldi et al. 2019; Jodry et al. 2019). These approaches were however tested mainly for relatively limited investigation lengths and increasing the survey lengths can pose limitation in most commercial tomographic software.

Data acquisition with streamer systems may indeed provide large datasets in short time. The amount of data requires automatic processing techniques to be implemented and parsimonious inversion methods. For DC curves extraction several automatic picking approaches were proposed in the literature and the number of available methods has exponentially raised in recent years (e.g. Zhinong et al. 2021; Colombero et al., 2022; Hui et al. 2024; Pace et al., 2024; Mengyuan et al. 2025; Xingjian et al. 2025; Xiaoping et al. 2025). Nevertheless, most of these approaches were verified on synthetic data and on few experimental data, often specifically acquired. With this respect, the availability of an independent dataset, acquired for production purposes, could offer the basis for the validation of the different automatic DC picking algorithms.

Most of the developed interpretation approaches of both resistivity and seismic data rely on the evaluation of the geophysical parameters along longitudinal sections of the investigated embankment through specific inverse problem solution. Given the aim of using geophysical data as a fast characterization tool, innovative approaches based on direct data transformations have also been developed, particularly for seismic data (e.g. Comina et al. 2020a; Comina et al. 2022; Lu et al. 2023). Beside the estimation of Vs, seismic records can also be used to compute energy attributes that allow for detection and location of local anomalies directly (e.g. Nasseri-Moghaddam et al. 2005; Zerwer et al.

https://doi.org/10.5194/essd-2026-32
Preprint. Discussion started: 3 March 2026

2005; Bergamo and Socco 2014; Colombero et al. 2019). Even though these last methods do not provide physical parameters to be correlated with geotechnical properties, they can be very useful for the identification of the anomalous zones of the embankment to be further assessed through in situ geotechnical testing.

Finally, the 3D shape of the embankment can partially affect the geophysical data interpretation and could strongly influence the results of both resistivity and seismic interpretations (e.g. Sjödahl et al. 2006; Hojat et al. 2019; Karl et al. 2011). Therefore, 3D effects should be considered in some specific conditions, even if there is still no standardized approach in their interpretation and in the way these effects should be taken into account. For this reason, more datasets are necessary to test and benchmark different inversion attempts or approximate data transformations.

We here present a dataset of a 4 km combined seismic and electric streamer survey along the embankment of the Po River in Crescentino, near Torino, in north-west Italy. Data acquisition strategies with the use of an appropriate seismic and electric streamer cable are discussed and preliminary data analyses are reported. All the acquired geophysical data are described in the paper, organized in a structured dataset and commented in detail in the attached files concerning their format and organization. Complementary geotechnical and topographic information are also included in the dataset as essential data for comparison. The whole dataset is made available (https://doi.org/10.5281/zenodo.18183049) for benchmarking alternative processing and interpretation approaches.

2 STUDY SITE, GEOTECHNICAL AND TOPORAPHIC DATA

The investigated test site is the Crescentino embankment of the Po River, near Torino, in north-west Italy (Figure 1). This embankment was built to protect the village of Crescentino and its surroundings, industrial and agricultural activities, from Po river floods. The embankment recently underwent maintenance interventions due to localized seepages, particularly in its terminal eastern portion, nearer to the Crescentino village (Figure 1).

Available geotechnical data and on purpose acquired topographic data are hereafter described and included in a specific qgis project (QGIS_topography/Database.qgz). For geotechnical tests, 7 Dynamic Probing Super Heavy (DPSH) tests and two boreholes logs,

https://doi.org/10.5194/essd-2026-32
Preprint. Discussion started: 3 March 2026

Open Access Earth System Science Data Discussions

are included in the project, in numeric format for DPSH and in stratigraphic representation for the borehole logs. For topographic data an on purpose acquired Digital Terrain Model (DTM) and orthomosaic of the embankment are also included.

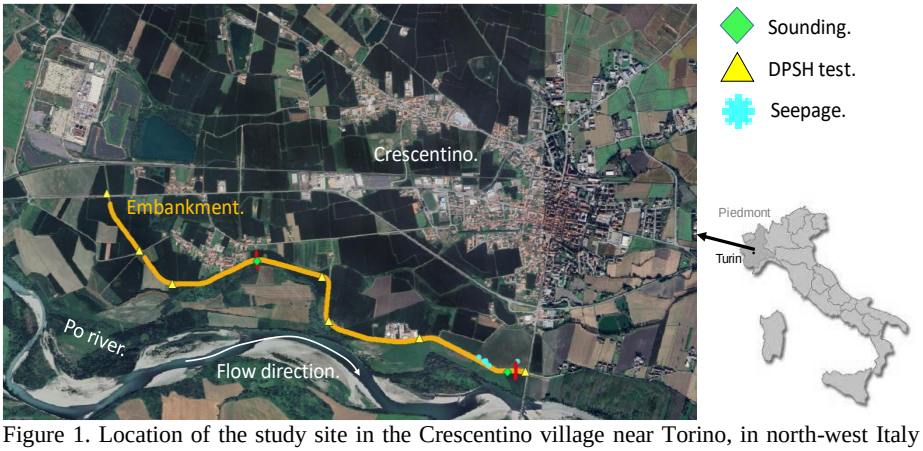

Figure 1. Location of the study site in the Crescentino village near Torino, in north-west Italy (inlet), with evidence of the available geotechnical tests and seepage phenomena along the embankment, in red the position of the sections reported in Figure 2 is evidenced (Map data ©2023 Google, acquired from Airbus).

2.1 geotechnical data

Available borehole logs (Figure 2) over the embankment report a variable subsoil structure whose principal elements are:

- Embankment body (3 to 6 m thick): constituted of natural material from the surroundings, mainly loose, medium-fine, grey-brown sand with rounded to angular polygenic centimetric gravels and centimetric pebbles; the gravel content in the embankment is higher in the western portion than in the eastern one;
- Fondation soil (5 to 10 m thick): constituted of rounded, polygenic centimetric gravels and centimeter-sized pebbles in a sandy matrix of medium-coarse, brownish-gray color; localized intercalations of dark gray, slightly compacted silty sand with rounded to angular polygenic centimeter-sized gravels and centimeter-sized pebbles were also observed;
- Geological substratum (locally evidenced only in the eastern portion of the embankment from 10 m depth): marls ranging from gray-brown to light brown with bluish-gray mottled streaks and abundant centimetric carbonate concretions.

https://doi.org/10.5194/essd-2026-32
Preprint. Discussion started: 3 March 2026

In the two available borehole logs the water table is identified at about 5 and 3.5 m depth in the western and eastern parts respectively, showing a slight lowering from west to east, coherently with the Po river flow direction and the attended hydrogeological setting.

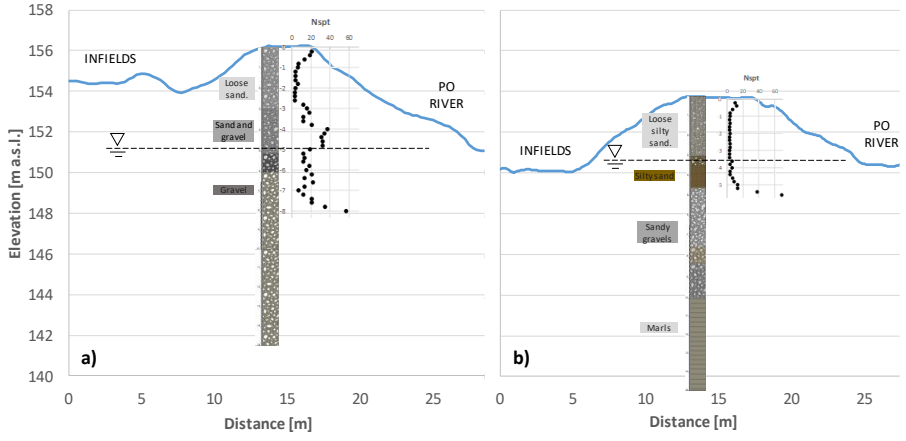

Figure 2. Schematic representation of the shape and geotechnical properties along the a) western and b) eastern portions of the Crescentino embankment, for the location of the sections refer to Figure 1.

Dynamic Probing Super Heavy (DPSH) tests also report variable data along the embankment:

- A shallow (about 0.5 m) top portion of the embankment, corresponding to the gravelly service road, with medium-high DPSH counts (10 to 15);
- The embankment body: with low DPSH counts (less than 5), particularly in the eastern portion of the embankment, or locally higher DPSH counts (above 10) in the western portion;
- The foundation soil with high DPSH counts (generally higher than 20) but with local intercalation of reduced blow counts layers.

The embankment has a variable height along its extension. In Figure 2 we show two representative cross-sections located in correspondence of the available borehole logs, and representative DPSH results in the nearby. These sections well represent the variability of construction materials observed along the embankment with the western portion being generally coarser and more compacted (increased gravel content and higher DPSH counts) than the eastern portion, finer and looser (lower gravel content and reduced DPSH counts).

https://doi.org/10.5194/essd-2026-32
Preprint. Discussion started: 3 March 2026

The above described lateral variability is also reflected in a different construction design among the two portions of the embankment (Figure 3). In the western portion (Figure 3a) the river side of the embankment was protected in its terminal part with a concrete slab reinforced with an electro welded mesh, and a short (less than 2 m deep) diaphragm at the toe. Conversely, in the eastern portion the actual structure (Figure 3b) is the result of maintenance interventions and rising of the older embankment adopted to prevent seepage. Here, the river side of the embankment was covered with a metal mattress, made by a heavily galvanized net, filled with medium-sized stones. Furthermore, 5 to 6 m deep jet grouting columns were executed at the toe of the older embankment to reach the marl substratum.

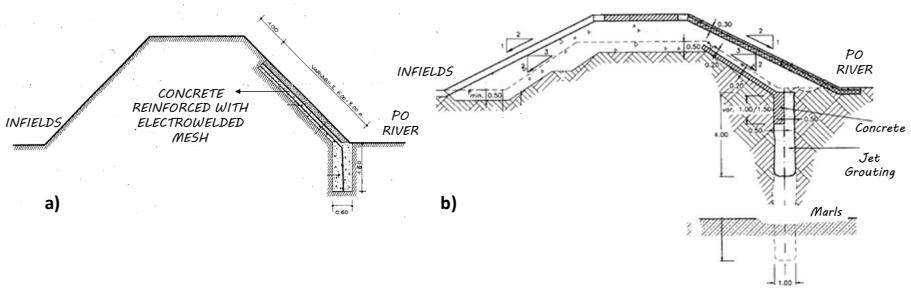

Figure 3. Construction designs adopted along the a) eastern and b) western portions of the Crescentino embankment.

Both the adopted design approaches can introduce 3D effects and may cause artefacts in the geophysical data analyses if interpreted in a 2D approach. Therefore, the availability of the above construction details could be very useful for benchmark different elaboration approaches.

2.2 Topographic data

The example sections reported in Figure 2 and the general topographic data along the embankment were obtained from an on-purpose acquired DTM with associated orthomosaic through an Unmanned Aerial Vehicle (UAV) survey. The survey flight was optimized for the long and narrow shape of the embankment by running a single swipe along it, with no lateral overlapping. This approach was attempted to evaluate its effectiveness over similar case studies, in order to reduce the survey time and costs where no transversal extension is needed.

https://doi.org/10.5194/essd-2026-32
Preprint. Discussion started: 3 March 2026

A total of 22 photogrammetric targets were homogeneously distributed along the survey path, both on the top of the embankment and at the base of the slopes, serving as Ground Control Points for the georeferencing of the point cloud. The GPS position of the targets were taken with a RTK GNSS antenna (Emlid Reach RS3) and given in absolute coordinates in the UTM WGS84 system, Fuse 32N.

The UAV survey consisted in total of 243 images, taken from an elevation of about 90 m, with a minimum overlap of 5 to 6 images in the central part. The total covered area by the survey was of about 0.5 square kilometres, with a ground resolution of 3 cm/pixel. The photogrammetric survey was performed with the DJI Mavic Pro 3T drone, controlled with the mission planning software UgCS Pro (SPH Engineering, Latvia). A focal length of 24 mm, an image resolution of 4000x3000 pixels and a pixel size of 1.59 micrometers were adopted. The processing workflow, implemented in Metashape Professional software (Agisoft), was based on the generation of a point cloud from a structure-from-motion algorithm and can be schematized as follows: alignment of all the acquired images; creation and filtering of the sparse point cloud; georeferencing of the point cloud with the photogrammetric targets; creation of the dense point cloud, of the mesh and texture; output creation (orthomosaic and DTM).

The accuracy of the photogrammetric model, necessary for the estimation of the overall errors in the generated point cloud, was estimated by selecting some of the targets as Check Points. The average X error was 3.46 mm, the average Y error was 5.6 mm, the average Z error was 2. 45 mm.

3 GEOPHYSICAL DATA

Seismic and electrical resistivity measurements were executed along the embankment by means of a combined seismic and electric streamer cable (Figure 4a and b). The streamer integrates seismic receivers and electrodes with a deployment that optimizes resolution, investigation depth and acquisition efficiency. For the seismic part, the streamer is constituted by 48, 4.5 Hz vertical geophones at 1 m spacing. The seismic source is a 40 Kg accelerated mass mounted on the survey vehicle (Figure 4c). The first geophone is placed at a 6 m offset from the source. For the electric part, the streamer is similar to what reported in Arato et al. (2022) and is constituted by 13 active electrodes, that can be used both as current and potential electrodes, placed at increasing spacings around their mid-

https://doi.org/10.5194/essd-2026-32
Preprint. Discussion started: 3 March 2026

point (Figure 4b). The shorter spaced electrodes are those located around the streamer mid-point (7 electrodes at 2 m separation), while the farthest spaced ones are at the extremities of the streamer (8 m separation). Electrodes are constructed in stainless steel and have the form of brushes (Figure 5a), to increase the contact surface to the ground and reduce coupling resistances. A drip irrigation system completes the electric part of the streamer to further reduce contact resistances at the electrodes. Details of the electrodes, the irrigation system and the resulting effect of their use over the investigated embankment are shown in Figure 5.

The resulting streamer total length is of about 50 m. The seismic and electric streamer is dragged by the survey vehicle (Figure 4c) that carries the equipment for seismic and electric resistivity measurements (acquisition systems and water tank). The electrodes and geophones are connected to the acquisition systems (Syscal-Pro, Iris Instruments, georesistivimeter and DaQLink IV, Seismic Source, seismic recording system) by means of multipolar cables. Cables and the irrigation system are collected all together in a plastic coating for easier dragging (Figure 4a).

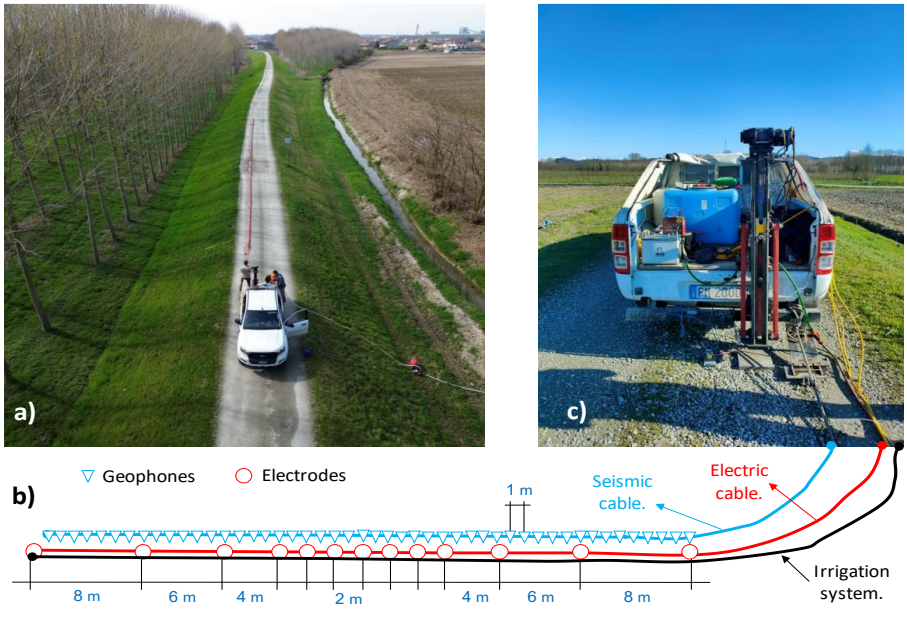

Figure 4. Seismic-electric streamer survey: a) picture of the seismo-electric streamer dragged by the survey vehicle during data acquisition, b) scheme of the streamer with evidence of geophones and electrodes disposition and c) picture of the survey vehicle with equipment necessary for seismic and resistivity measurements.

https://doi.org/10.5194/essd-2026-32
Preprint. Discussion started: 3 March 2026

Figure 5. Seismic-electric streamer survey: a) detail of the adopted electrodes and irrigation system and b) the resulting effect of their use over the investigated embankment.

3.1 Survey design and data acquisition

The streamer is dragged along the embankment and measurements are carried out at 8 m steps; at each moving step, a single seismic shot and an electric resistivity acquisition sequence are recorded. The survey step was chosen according to simulations as the best compromise between lateral resolution and acquisition efficiency. Specifically, given that the acquisition of electric data is the most time consuming for the surveys, the 8 m value was adopted through numerical simulations of the electrical resistivity surveys.

To this aim several forward modelling tests were performed on a simulated 2D model of the embankment, with a background resistivity of 100 Ohm.m and 10 Ohm.m conductive square-shaped anomalies, with a side length of 1m, placed at several depths (every 1 m). These anomalies are intended to represent higher porosity areas potentially leading to dangerous seepages. Different acquisitions were simulated with custom 13-electrodes quadrupole sequences in order to evaluate obtainable resolution and investigation depth. The different quadrupole sequences were designed focusing on speed, therefore including fewer measurements than a standard sequence. Specifically we prioritized: Dipole-Dipole (DD) measurements with adjacent current electrodes, to allow delineate lateral variations; Wenner-Schlumberger (WS) measurements with small current electrodes spacing, to obtain robust measurements near the surface, and because they can be easily linked to DD measurements (using external potential electrodes) and performed simultaneously by the multi-channel instrument; WS measurements with larger current electrodes spacing, for robust deeper measurements.

The finally chosen acquisition sequence used both WS and DD quadrupoles and consisted of a total of 318 electric potential readings. In the end, we also checked that the points of

https://doi.org/10.5194/essd-2026-32
Preprint. Discussion started: 3 March 2026

the pseudosections of adjacent acquisitions (after moving the streamer each time by the measurement step), were distributed homogeneously. This can be observed in Figure 6 for three consecutive acquisition sequences at increasing station positions. It can be noted that a high data density is obtained within the first 5 m of depth, with a very good vertical and lateral resolution, while the data density progressively decreases with depth.

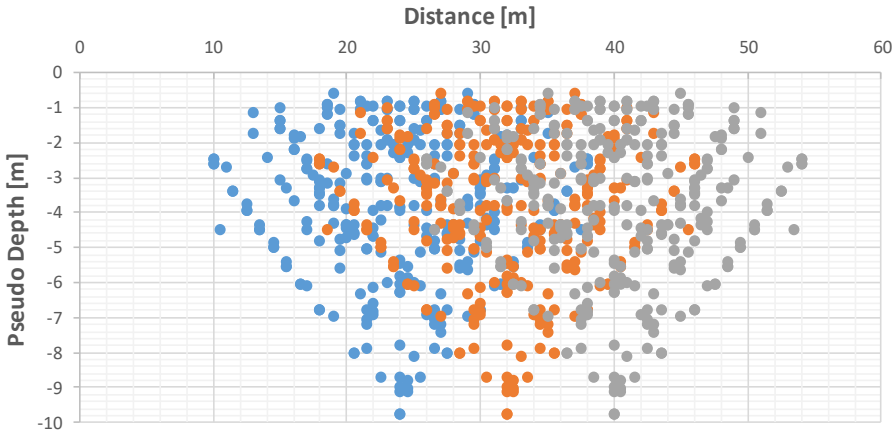

Figure 6. Example electric acquisition: pseudo depth representation of three consecutive acquisition sequences at increasing station positions.

In Figure 7 an example result of the simulations obtained with the finally chosen acquisition sequence and with 4 m and 8 m advancement steps of the streamer system are reported. It can be noticed that no meaningful differences in detecting targets in the first 5 meters of depth are observable. The 4 m step acquisition performs only slightly better at greater depths due to increased data coverage of the deeper quadrupoles (see also Figure 6). However, since the 8 m advancement step halves the acquisition time, it was considered a better option, notwithstanding the slight loss in resolution with depth, also considering the attended embankments heights in the survey.

From the seismic data point of view, the influence of the acquisition step is instead less problematic. Seismic data can take advantage of the denser geophones distribution along the streamer and even a 8 m advancement step (corresponding to the shot spacing), as the one adopted in the surveys, does not compromise lateral resolution. As an example MASW data elaboration and DC extraction can be performed even at 1 m separation by considering an appropriate geophone moving window and stacking the far offset shots. A preliminary example of seismic data elaboration is reported later in the paper.

https://doi.org/10.5194/essd-2026-32
Preprint. Discussion started: 3 March 2026

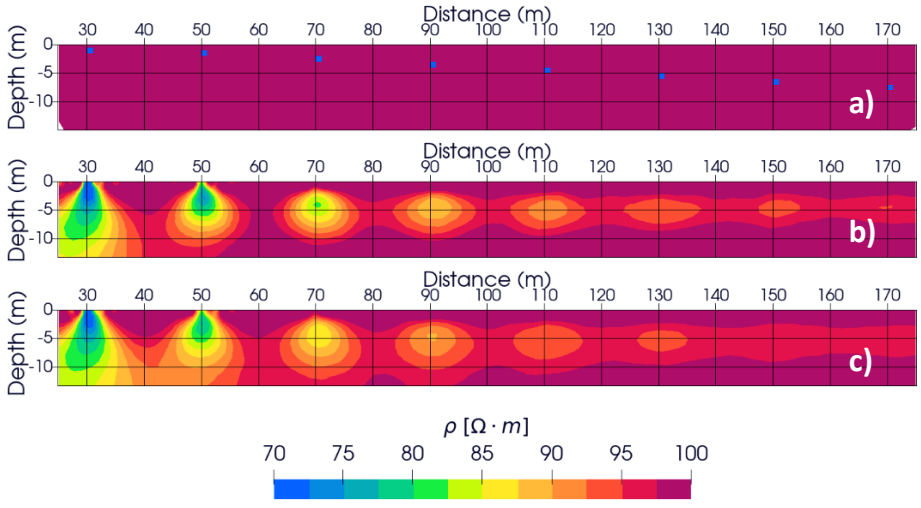

Figure 7. Numerical simulations of electrical resistivity surveys over several square-shaped conductive anomalies: a) position of anomalies; resulting resistivity models simulating an acquisition with streamer advancement step of 4 m b) and 8 m c).

At each station position the location of the electrode nearest to the survey vehicle (which correspond also to the first geophone) was acquired by means of a RTK GNSS antenna (Emlid Reach RS3). In specific positions, particularly in correspondence of embankment curves with a narrower radius, additional GPS data were also acquired along the streamer in its central and terminal parts. These last data, not included in the database, allowed a very reliable positioning of all the electrodes and geophones of the survey (see later). The position data are made available in the qgis project (/QGIS_topography/Stations.gpkg) in absolute coordinates in the UTM WGS84 system, Fuse 32N (Figure 8). Position data are numbered starting from the western part of the embankment, as acquired during survey acquisition.

During a 7 days' survey campaign, 518 station positions were acquired (Figure 8), with productivity of 800 m/day and about 15 stations per hour of effective acquisition. A relevant amount of time was necessary to deploy and recollect the streamer each day and to refill the water tank for the drip irrigation system. The acquired data provided a continuous coverage of the investigated embankment apart from a small portion of about 50 m in the eastern part (Figure 8) related to the crossing of a road which prevented the positioning of the streamer.

https://doi.org/10.5194/essd-2026-32
Preprint. Discussion started: 3 March 2026

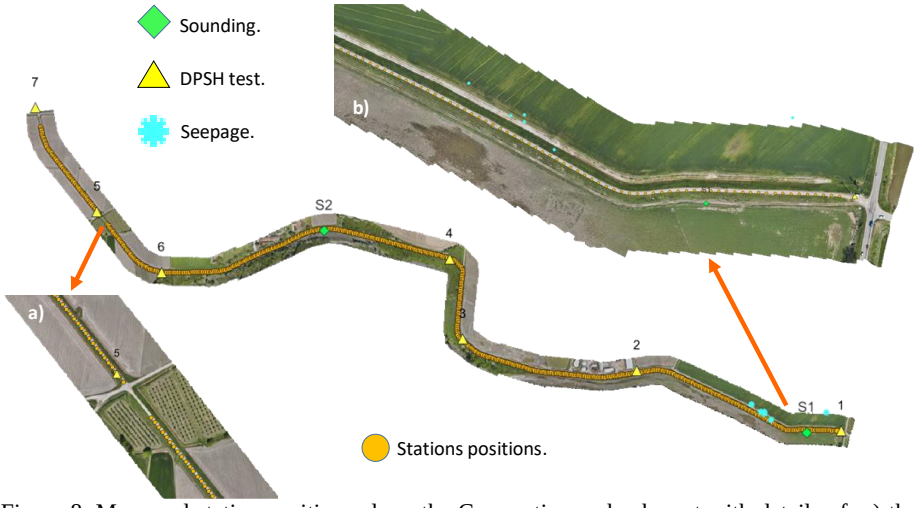

Figure 8. Measured station positions along the Crescentino embankment with details of: a) the small portion of about 50 m in the eastern part with no data and b) the data acquired in the terminal western portion.

3.2 Seismic data

All the acquired seismic gathers are reported in the database (/Seismic_Survey_Data/) in SEG2 format. Files are ordered using a progressive number from 1, on the western part of the embankment, to 518, in the eastern one. Seismic data were acquired with a 0.5 ms sampling rate, a 0.05 s pretrigger and a 1 s record duration. An example seismic shot is reported in Figure 9.

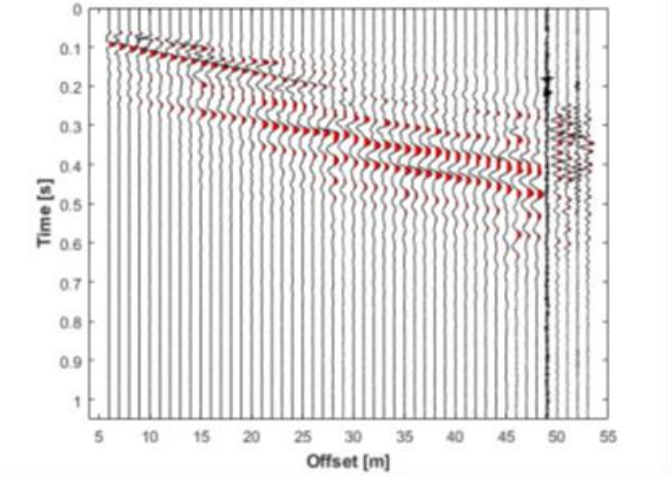

Figure 9. Example seismic acquisition: seismic shot with evidence of malfunctioning geophones at the end of the streamer.

https://doi.org/10.5194/essd-2026-32
Preprint. Discussion started: 3 March 2026

Data were generally of good quality with just few geophones showing low quality coupling. At some specific locations seismic shots were repeated due to the presence of external disturbances (e.g. tractors and cars). During the first survey days some of the geophones showed malfunctioning (Figure 9 – geophones above number 49). These were moved at the end of the streamer to not compromise the whole seismogram and were later substituted.

Starting from the measured GPS positions (Figure 8) the location of each geophone along the streamer was extrapolated using a continuous polyline. The locations of each geophone along the streamer are also included in the database in a specific .csv file (/Seismic_Survey_Data/geophones_positions.csv) ordered as in the acquisition.

3.3 Electric resistivity data

The optimization of quadrupole measurement protocol (for both DD and WS quadrupoles) allowed to perform the 318 electric potential readings sequence with only 34 current injections in about one minute, with the addition of few gap-fillers. For each new station position, contact resistances at electrodes were verified; in case of high contact resistances, the drip irrigation was continued till a satisfactory value. This last step increased the acquisition time and occurred generally over the gravellier portions of the road on the embankment.

During acquisitions, the current injection time was of 250 ms in each current dipole and the measurements were stacked 3 times; in case of standard deviation greater than 2%, the measurements were stacked 6 times instead.

All the acquired electric resistivity data are reported in the database (/Electrical_Tomography_Data/Resistivity_data.csv) in .csv format with indication of the measuring electrodes and the data type of each acquisition. A total of 164724 potential readings were acquired in the 518 executed station positions. Following the same approach previously adopted for the seismic data the location of each electrode along the streamer for each station position was also computed. These latter are also available in the database in a specific .csv file (/Electrical_Tomography_Data/Electrodes_Positions.csv) ordered as in the acquisition.

https://doi.org/10.5194/essd-2026-32
Preprint. Discussion started: 3 March 2026

4 PRELIMINARY DATA ANALYSES

Preliminary analyses were performed on the above described data to provide a first visualization of the Vs and resistivity distributions along the embankment and discuss the potential use of the data also with alternative interpretation approaches. The analyses commented and reported hereafter are not directly included in the database which is focused specifically on the raw data. Authors are however available to share and further compare specific data analyses upon requests.

4.1 Seismic data

We estimated Rayleigh wave fundamental mode DCs for the whole seismic dataset. An automatic approach for DC extraction, based on the selection of a predefined searching area in the dispersion image, was adopted (Figure 10) and the results were compared with some sample manually picked DCs to check the reliability of the automatic picking. The DCs were picked as the maxima of phase velocity-frequency spectra (Park et al., 1998) computed for a moving window of 24 receivers (the nearest to the shot position) and stacking the spectra from 3 consecutive shots.

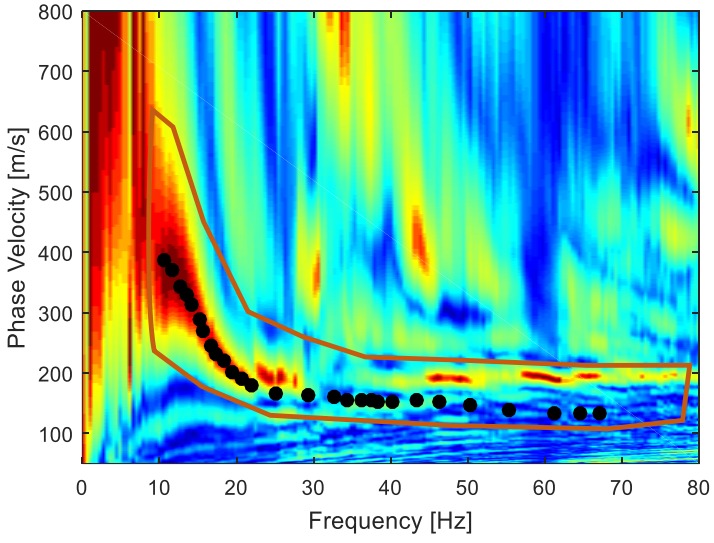

Figure 10. Example of dispersion image from the stacking of 3 consecutive shots. Brown box bounds the adopted search area; black dots corresponds to the manually picked DC.

https://doi.org/10.5194/essd-2026-32
Preprint. Discussion started: 3 March 2026

Different combinations of shots and number of geophones were also attempted observing that for an increasing number of geophones the quality of the dispersion image worsen, probably due to a lateral variability along the embankment. The automatic and manually picked DCs are not included in the database but will be available upon request to database users to compare with their DC extraction approaches.

Figure 10 shows an example of Dispersion image with the picked DC. As it can be observed higher modes are dominant in the dispersion image in the higher frequency band. This effect is quite common over embankment structures due to the presence of the compacted road above it or to 3D effects linked with the geometry of the embankment. The presence of these higher modes can affect the automatic DC extraction.

A reliable analysis of the DC was possible in the 10 to 60 Hz frequency band for most of the shots. Given the velocity ranges of the investigated materials (see Figure 10) this frequency band correspond to maximum and minimum wavelengths of about 30-40 m and 2 m respectively. Given these ranges it can be therefore considered that the investigation depth of the seismic survey is slightly higher than the one of resistivity surveys and with a comparable resolution at shallower depths.

4.2 Electric resistivity data

Electric resistivity data were analysed to remove anomalous apparent resistivity values. Data having negative resistivities, outliers (data with very high or very low resistivity, and isolated) and few data having higher standard deviation were removed. This result in about 10 % of the acquired measurements to be rejected.

Preliminary 2D and 3D inversions were also attempted on a small portion of the electric resistivity dataset by means of the Resipy software (Blanchy et al. 2020). For 3D inversion the shape of the embankment and the exact location of the electrodes was properly considered from the available topographic data.

5 DATA VISUALIZATION AND DISCUSSION

Figure 11 shows the filtered apparent resistivity data presented in the form of a pseudo section and the DCs represented in the form of 1D time average Vs models. The time average Vs models were estimated by directly transform the DCs through a linear wavelength-depth transformation (W-D transform) proposed by Comina et al. (2022) on the basis of the analysis of a wide flat-file database of surface waves dispersion curves

https://doi.org/10.5194/essd-2026-32
Preprint. Discussion started: 3 March 2026

and Vs profiles (Passeri et al., 2021). Both pseudo sections were obtained by gridding the experimental data with a kriging interpolation in a grid of 1 m vertical spacing and 10 m horizontal spacing. The available geotechnical and borehole information along the embankment is superimposed to the geophysical data and the location of known seepage events is also reported. Also, the estimated embankment depth is visualized over the other data.

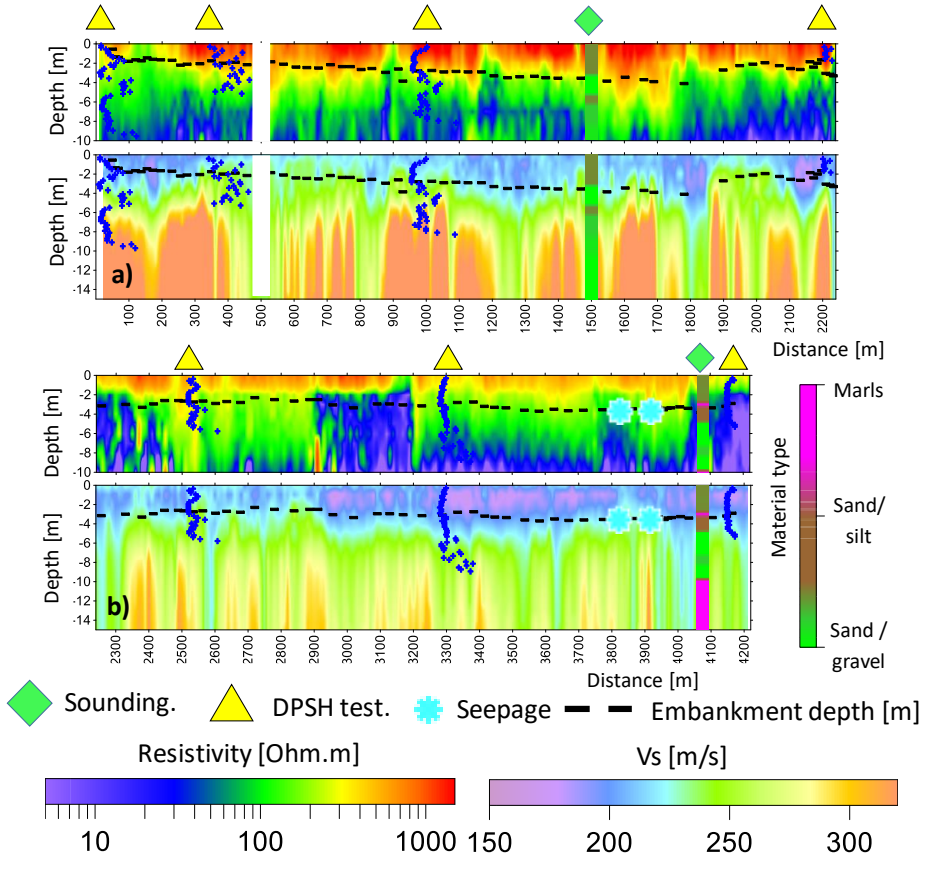

Figure 11. Visualization of the resistivity and time average Vs data along the western a) and estern b) portions of the embankment together with available geotechnical information and evidence from localized seepages.

From these preliminary data visualization, it can be evidenced that the lateral variability along the embankment evidenced by the geotechnical investigations is correctly depicted by geophysical data and that the there is a good correspondence with the information from geotechnical investigations.

https://doi.org/10.5194/essd-2026-32
Preprint. Discussion started: 3 March 2026

Along the western part (Figure 11a) the embankment is generally characterized by high resistivity values (above 800 Ohm·m) and medium-high velocity values (generally higher than 200 m/s), indicating the presence of mainly medium compacted sands inside it. Below the embankment a decrease in resistivity related to the presence of the water table is observed, and an increase in velocity due to the gravellier nature of the subsoil. Specifically, the marked increase in velocity (above 300 m/s) well correspond with the evidence from DPSH tests.

Conversely, along the eastern part (Figure 11b), the embankment is generally characterized by medium resistivity values (300 to 800 Ohm·m) and generally lower velocity values (lower than 200 m/s) indicating the presence of mainly medium loose silty sands inside it. Below the embankment, a decrease in resistivity similar to the western part is observed. However, a less sharp increase in velocity is noted which may be related to the lateral transition from gravels to compacted marls (substratum).

Some localized low resistivity and low seismic velocity areas emerge from the surveys. These areas could be potentially related to critical portions within the embankment and shallow foundation soil, characterized by increased water content (low resistivity data) and reduced compactness (low seismic velocity).

The data visualization proposed in Figure 11 offers a fast and simple way to picture the embankment conditions. This can be beneficial in situations in which a fast preliminary evaluation of the state of health of an embankment is required (e.g. in the case of surveys conducted near, or in foresee of, significant rain and/or flood events). In these conditions, the proposed data acquisition and visualization approach can allow an almost immediate evaluation of geophysical parameters distribution at the site and a direct imaging of the resistivity and seismic properties, even while the acquisition is in progress, during the dragging of the streamer along the embankment.

To better pinpoint localized anomalies, the analysis of seismic data was also complemented with the computation of the Energy (Ei) and Autospectral Density (ADi) of all the acquired seismic traces along the profile. These data attributes showed both in numerical simulations and in real case histories their ability in detecting and locating anomalies having lower acoustic impedance than the surrounding material (Colombero et al. 2019). These type of anomalies is usually observed with an increase in both Ei and ADi and could be related to potential weakness zones along the embankment. In Figure

https://doi.org/10.5194/essd-2026-32
Preprint. Discussion started: 3 March 2026

12 we display these attributes along the embankment. For the ADi the same wavelength to depth conversion used for the DC was adopted to transform the frequency in an estimated depth. To allow better understanding of the lateral variations, both the parameters were normalized along the whole embankment length.

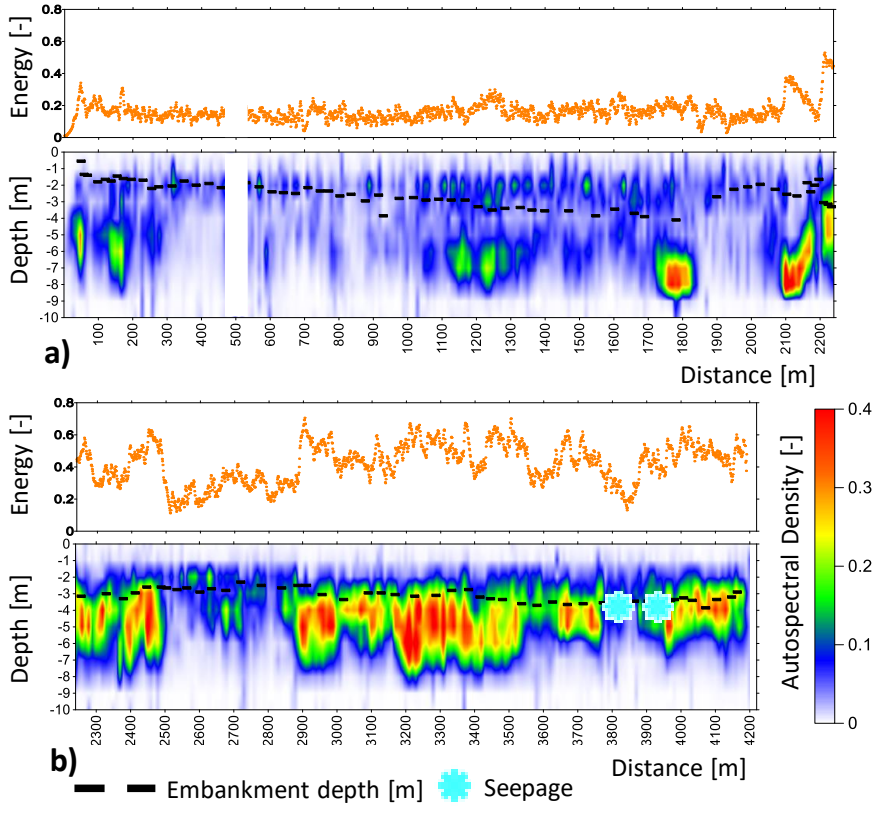

Figure 12. Normalized Energy (top) and Autospectral Density (bottom) of all the acquired seismic traces along the western a) and eastern b) portions of the embankment together the evidence from localized seepages.

The different properties of the western and eastern parts of the embankment are confirmed also by this analysis. Indeed, along the western part (Figure 12a) low Ei values and few localized high ADi spots are evidenced, indicating a generally uniform condition and few anomalies. Conversely along the eastern part (Figure 12b) several high Ei peaks and high ADi spots are evidenced. Particularly from the progressive 2900 m on localized seepages are well known within the embankment and could be the cause for the anomalies in the seismic parameters.

https://doi.org/10.5194/essd-2026-32
Preprint. Discussion started: 3 March 2026

Notwithstanding the good correspondence observed between geophysical data and geotechnical information, some of the evidenced anomalies need to be further investigated since they may be related to 3D effects near embankment curves or specific embankment design features. In Figure 13 the results of the 2D and 3D inversions of resistivity data in a 1 km portion of the embankment are reported and compared to the measured pseudosection. The investigated portion is located between progressives 2100 and 3100 in correspondence to a significant embankment curve (i.e. at the position of DPSH 3 in Figure 8).

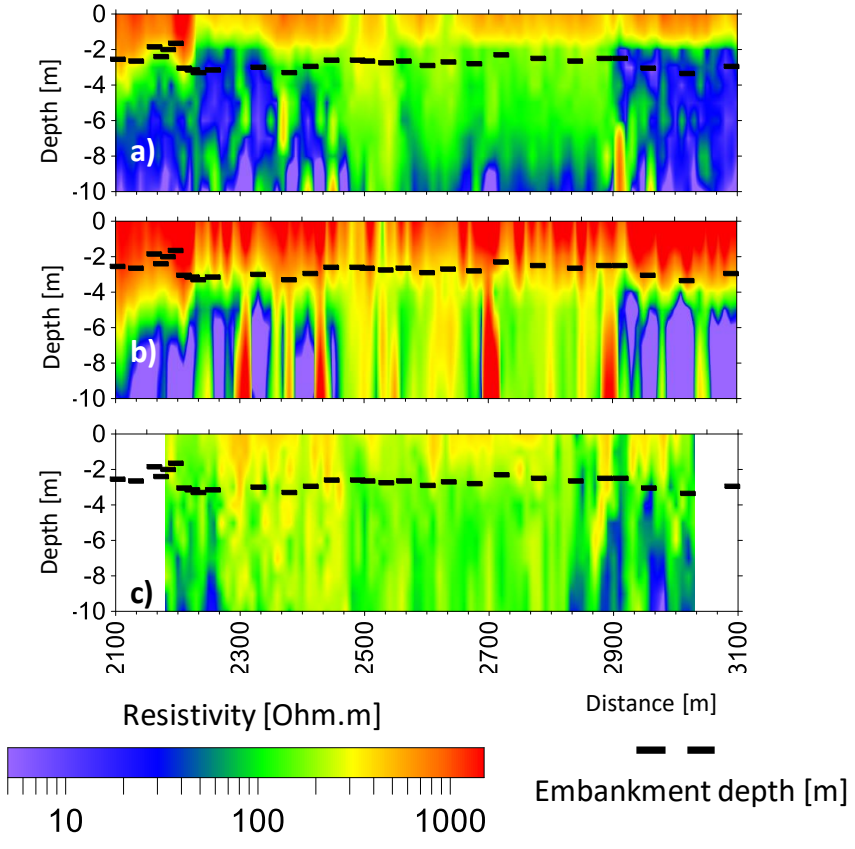

Figure 13. Resistivity data inversion over a small portion of the embankment between progressives 2100 and 3100 m in correspondence to a significant embankment curve (i.e. DPSH 3 in Figure 8): comparison between a) pseudo section b) 2D and c) 3D inversions.

From this analysis it can be evidenced that even if the general resistivity distribution is quite similar between pseudosection, 2D and 3D inversions some differences related to the different processing approaches emerge. Specifically, 2D inversions tend to provide

https://doi.org/10.5194/essd-2026-32
Preprint. Discussion started: 3 March 2026

a result with sharper resistivity contrasts, while the 3D inversion provides a smoother image reducing the resistivity contrasts below the embankment. Therefore, as already evidenced in literature (e.g. Sjödahl et al. 2006; Hojat et al. 2019) when the aim of the survey is the definition of potential correlation between resistivity data and geotechnical parameters, the use of 3D inversion is to be considered mandatory for an appropriate quantification.

Similar and more detailed data analyses than the one here presented could be object of further studies on both electric and seismic datasets. For example, with respect to seismic data also the compressional wave velocity distribution could be investigated with first break picking tomographic approaches or with devoted data transform approaches from the same DCs (e.g. Comina et al., 2020a). For electric data, 3D inversions with the inclusion of a-priori information related to the embankment design and structure (Figure 3) could be also attempted for a better understanding of lateral effects.

6 CONCLUSION

The use of combined seismic and electric streamer surveys for the characterization and screening of embankments also for relevant investigation lengths was shown in this work. The executed surveys allowed to cover the whole investigated embankment in relatively short acquisition times, providing information on the distribution of the geophysical parameters. A comprehensive dataset of the acquired electrical resistivity and seismic data was built, including also independent geotechnical and topographic information. The dataset is made available for benchmarking alternative processing and interpretation approaches in order to contribute to the advancement of the state of the art of these characterization methodologies. Further data processing and inversion are foreseen in the near future for a more complete characterization together with combined resistivity and seismic analyses with the aim of specific geotechnical parameters estimation.

https://doi.org/10.5194/essd-2026-32
Preprint. Discussion started: 3 March 2026

Acknowledgments

This study was carried out within the GEOCHARME project – funded by the European Union – Next Generation EU within the PRIN 2022 program (D.D. 104 - 02/02/2022 Ministero dell'Università e della Ricerca). This manuscript reflects only the authors' views and opinions and the Ministry cannot be considered responsible for them.

Authors are indebted with AIPO – Moncalieri section for support in the identification of relevant case histories for the project and for the sharing of independent geotechnical data.

Field data acquisition was also supported by Techgea Srl within the GEOLEVEE Project, funded by the "Return - Multi-Risk sciEnce for resilienT commUnities undeR a changiNg climate" program (PNRR, Missione 4 "Istruzione e ricerca" – Componente 2 "dalla ricerca all'impresa", Investimento 1.3, finanziato dall'Unione europea – Nextgeneration EU, pubblicato dal Politecnico di Milano con Decreto del Direttore Generale D.D. Rep. n. 7881/2024, Prot. n. 161661/2024 del 02/07/2024).

Data Availability

All the data described in the paper are available in a structured dataset at: Vergnano, A., Comina, C., Socco, L. V., Chieppa, D., & Arato, A. (2026). Database of a 4-km seismic and electric streamer survey: the embankment of the Po River near Crescentino, Piedmont, Italy. [Data set]. Zenodo. https://doi.org/10.5281/zenodo.18183049.

REFERENCES

Bergamo, P., and L. V. Socco, 2014, Detection of sharp later discontinuities through the analysis of surface-wave propagation: Geophysics, 79, no. 4, EN77-EN90.

Blanchy, G., Saneiyan, S., Boyd, J., McLachlan, P., Binley, A., 2020. ResIPy, an intuitive open source software for complex geoelectrical inversion/modeling. Comput. Geosci. 137, 104423.

Borgatti, L., Forte, E., Mocnik, A., Zambrini, R., Cervi, F., Martinucci, D., Pellegrini, F., Pillon, S., Prizzon, A., Zamariolo, A., 2017. Detection and characterization of animal burrows within river embankments by means of coupled remote sensing and geophysical techniques: Lessons from River Panaro (northern Italy). Eng. Geol. 226, 277–289.

Brodic, B., Malehmir, A., Juhlin, C., Dynesius, L., Bastani, M., and Palm, H. (2015). Multicomponent broadband digital-based seismic landstreamer for near-surface applications. Journal of Applied Geophysics, 123, 227-241.

Busato, L., Boaga, J., Peruzzo, L., Himi, M., Cola, S., Bersan, S., Cassiani, G., 2016. Combined geophysical surveys for the characterization of a reconstructed river embankment. Eng. Geol. 211, 74–84.

An, N., Tang, C.S., Cheng, Q., Wang, D.Y., Shi, B., 2020. Application of electrical resistivity method in the characterization of 2D desiccation cracking process of clayey soil. Eng. Geol. 265.

Arato A., Vagnon F., Comina C., 2022, First application of a new seismo-electric streamer for combined resistivity and seismic measurements along linearly extended earth structures, Near Surface Geophysics, 20 (2), pp. 117 – 134.

Arosio, D., Munda, S., Tresoldi, G., Papini, M., Longoni, L., Zanzi, L., 2017. A customized resistivity system for monitoring saturation and seepage in earthen levees: Installation and validation. Open Geosci. 9, 457–467.

https://doi.org/10.5194/essd-2026-32
Preprint. Discussion started: 3 March 2026

Borgatti, L., Forte, E., Mocnik, A., Zambrini, R., Cervi, F., Martinucci, D., Pellegrini, F., Pillon, S., Prizzon, A., Zamariolo, A., 2017. Detection and characterization of animal burrows within river embankments by means of coupled remote sensing and geophysical techniques: Lessons from River Panaro (northern Italy). Eng. Geol. 226, 277–289.

Busato, L., Boaga, J., Peruzzo, L., Himi, M., Cola, S., Bersan, S., Cassiani, G., 2016. Combined geophysical surveys for the characterization of a reconstructed river embankment. Eng. Geol. 211, 74–84.

Colombero, C., Comina, C., Socco, L.V. Imaging near-surface sharp lateral variations with surface-wave methods - Part 1: Detection and location (2019) Geophysics, 84(6), pp. EN93–EN111.

Colombero C., Papadopoulou M., Kauti T., Skyttä P., Koivisto E., Savolainen M., Socco L.V. (2022) Surface-wave tomography for mineral exploration: A successful combination of passive and active data (Siilinjärvi phosphorus mine, Finland), Solid Earth, 13 (2), pp. 417 – 429.

Comina C., Vagnon F., Arato A., Antonietti A., Effective Vs and Vp characterization from Surface Waves streamer data along river embankments, 2020a, Journal of Applied Geophysics, 183, art. no. 104221.

Comina C., Vagnon F., Arato A., Fantini F., Naldi M., 2020b, A new electric streamer for the characterization of river embankments, Engineering Geology, 276, art. no. 105770.

Comina, C., Foti, S., Passeri, F., Socco, L.V. Time-weighted average shear wave velocity profiles from surface wave tests through a wavelength-depth transformation (2022) Soil Dynamics and Earthquake Engineering, 158, art. no. 107262.

Foti, S., Hollender, F., Garofalo, F., Albarello, D., Asten, M., Bard, P.-Y., Comina, C., Cornou, C., Cox, B., Di Giulio, G., Forbriger, T., Hayashi, K., Lunedei, E., Martin, A., Mercerat, D., Ohrnberger, M., Poggi, V., Renalier, F., Sicilia, D., Socco, L.V., 2018. Guidelines for the good practice of surface wave analysis: a product of the InterPACIFIC project. Bull. Earthq. Eng. 16, 2367–2420.

Hojat, A., Arosio D., Loke M.H., Longoni L., Papini M., Tresoldi G. and Zanzi L. (2019) Assessment of 3D geometry effects on 2D ERT data of a permanent monitoring system along a river embankment. Conference Proceedings, EAGE-GSM 2nd Asia Pacific Meeting on Near Surface Geoscience and Engineering, April, p. 1–15.

Hui Liu, Jing Li, Rong Hu, Automatic and adaptive picking of surface-wave dispersion curves for near-surface application, Journal of Applied Geophysics, Volume 221, 2024, 105282.

Ivanov, J., Miller, R.D., Lacombe, P., Johnson, C.D. and Lane, J.R. Jr. (2006) Delineating a shallow fault zone and dipping bedrock strata using multichannel analysis of surface waves with a land streamer. Geophysics, 71, A39–A42.

Jones, G., Sentenac, P., Zielinski, M., 2014. Desiccation cracking detection using 2-D and 3-D electrical resistivity tomography: Validation on a flood embankment. J. Appl. Geophys. 106, 196–211.

Jodry, C., Palma Lopes, S., Fargier, Y., Sanchez, M., Côte, P., 2019. 2D-ERT monitoring of soil moisture seasonal behaviour in a river levee: A case study. J. Appl. Geophys. 167, 140–151.

Karl, L., Fechner, T., Schevenels, M., François, S. and Degrande, G. (2011) Geotechnical characterization of a river dyke by surface waves. Near Surface Geophysics., 9, 515–527.

Lane Jr. J.W., Ivanov J., Day-Lewis F.D., Clemens D., Patev R. and Miller R.D. 2008. Levee evaluation using MASW: Preliminary findings from the Citrus Lakefront Levee, New Orleans,

https://doi.org/10.5194/essd-2026-32
Preprint. Discussion started: 3 March 2026

611 Louisiana. 21st Symposium on the Application of Geophysics to Engineering and Environmental
612 Problems, Philadelphia, USA, Expanded Abstracts, 703–712.

613 Lee, B., Oh, S., Yi, M.J., 2020. Mapping of leakage paths in damaged embankment using
614 modified resistivity array method. Eng. Geol. 266.

615 Lu Xinglin, Wei Wang, Chaopeng Luo, Muyang Wu, Chao Yang, Xian Liao, Longhuan Liu,
616 Zhihong Fu, A rapid detection method of towed array seismic surface wave for leakage passage
617 of dyke-dam, Journal of Applied Geophysics, Volume 217, 2023, 105189.

618 Lutz K., Fechner T., Schevenels M., Stijn F. and Degrande G., 2011, Geotechnical
619 characterization of a river dyke by surface waves, Near Surface Geophysics, Volume9, Issue6,
620 Pages 515-527.

621 Mengyuan Hu, Yudi Pan, Tianxiang Wang, Yiming Wang, Automatic picking of surface-wave
622 dispersion curves with an image segmentation method, Journal of Applied Geophysics, Volume
623 233, 2025, 105615.

624 Min D.-J. and Kim H.-S. 2006. Feasibility of the surface-wave method for the assessment of
625 physical properties of a dam using numerical analysis. Journal of Applied Geophysics 59, 236–
626 243.

627 Moura, R.M. and Senos Matias, M.J. (2012) Geophones on blocks: a prototype towable geophone
628 system for shallow land seismic investigations. Geophysical Prospecting, 60(1), 192–1200.

629 Nasseri-Moghaddam, A., G. Cascante and J. Hutchinson, 2005, A new quantitative procedure to
630 determine the location and embedment depth of a void using surface waves: Journal of
631 Environmental and Engineering Geophysics, 10, 51-64.

632 Pace F., Khosro Anjom F., Karimpour M., Bolève A., Benboudiaf Y., Pournaki H., Socco L.V.,
633 (2024) Fast and semi-automatic S-wave and P-wave velocity estimations from landstreamer data:
634 a field case from the Middle East, Frontiers in Earth Science, 12, art. no. 1304593.

635 Park, C. B., Xia, J., and Miller, R. D., 1998, Imaging dispersion curves of surface waves on
636 multichannel record: 68th Ann. Internat. Mtg., Soc. Explor. Geophys., Expanded Abstracts, 1377-
637 1380.

638 Passeri F., Comina C., Foti S., Socco L.v. (2021) The Polito Surface Wave flat-file Database
639 (PSWD): statistical properties of test results and some inter-method comparisons, Bulletin of
640 Earthquake Engineering, 19, pages2343–2370.

641 Sjödahl, P., Dahlin,T. and Zhou, B. (2006) 2.5D resistivitymodeling of embankment dams to
642 assess influence from geometry and material properties. Geophysics, 71, G107–G114.

643 Tresoldi, G., Arosio, D., Hojat, A., Longoni, L., Papini, M., Zanzi, L., 2019. Long-term
644 hydrogeophysical monitoring of the internal conditions of river levees. Eng. Geol. 259.

645 Umezawa R., Motoharu Jinguuji and Toshiyuki Yokota, 2022, Characterization of a river
646 embankment using a non-destructive direct current electrical survey, Near Surface Geophysics,
647 2022, 20, 238–252.

648 Van Der Veen,M., Spitzer,R., Green,A.G. andWild, P. (2001) De-sign and application of towed
649 land-streamer system for cost-effective 2-D and pseudo-3-D shallow seismic data acquisition.
650 Geophysics, 66(2), 482–500.

651 Vagnon F., Comina C., Arato A., Chiappone A., Cosentini R.M., Foti S., 2022a, Geotechnical
652 Screening of Linear Earth Structures: Electric and Seismic Streamer Data for Hydraulic

https://doi.org/10.5194/essd-2026-32
Preprint. Discussion started: 3 March 2026

653 Conductivity Assessment of the Arignano Earth Dam, Italy, Journal of Geotechnical and
654 Geoenvironmental Engineering, 148 (12), art. no. 04022105.

655 Vagnon F., Comina C., Arato A., 2022b, Evaluation of different methods for deriving
656 geotechnical parameters from electric and seismic streamer data, Engineering Geology, 303, art.
657 no. 106670.

658 Vergnano, A., Comina, C., Socco, L. V., Chieppa, D., & Arato, A. (2026). Database of a 4-km
659 seismic and electric streamer survey: the embankment of the Po River near Crescentino,
660 Piedmont, Italy. [Data set]. Zenodo. https://doi.org/10.5281/zenodo.18183049

661 Xiaoping, H., Jiashun, Y., Jianlong, Y. et al. An automatic algorithm for surface wave dispersion
662 curve picking based on Hessian matrix attributes. Sci Rep 15, 21595 (2025).

663 Xingjian Kuang, Yudi Pan, Zeyi Zhang, Sanyi Yuan, Automatic picking of multimodal Rayleigh-
664 wave dispersion curves from multicomponent data with an energy-density-based clustering
665 method, Geophysical Journal International, Volume 243, Issue 1, October 2025, ggaf323,
666 https://doi.org/10.1093/gji/ggaf323

667 Zerwer, A., M. A. Polak and J. C. Santamarina, 2005, Detection of surface breaking cracks in
668 concrete members using Rayleigh waves: Journal of Environmental and Engineering Geophysics,
669 10, 295-306.

670 Zhinong Wang, Chengyu Sun, Dunshi Wu, Automatic picking of multi-mode surface-wave
671 dispersion curves based on machine learning clustering methods, Computers & Geosciences,
672 Volume 153, 2021, 104809.